

Resonance-Enhanced Vibrational Spectroscopy of Molecules on a Superconductor

Jan Homberg,¹ Alexander Weismann^{1,*}, Troels Markussen,² and Richard Berndt^{1,†}¹*Institut für Experimentelle und Angewandte Physik, Christian-Albrechts-Universität zu Kiel, 24098 Kiel, Germany*²*Synopsys Denmark, Fruebjergvej 3, Postbox 4, DK-2100 Copenhagen, Denmark*

(Received 16 February 2022; revised 13 April 2022; accepted 13 July 2022; published 7 September 2022)

Molecular vibrational spectroscopy with the scanning tunneling microscope is feasible but usually detects few vibrational modes. We harness sharp Yu-Shiba-Rusinov states observed from molecules on a superconductor to significantly enhance the vibrational signal. From a lead phthalocyanine molecule 46 vibrational peaks are resolved enabling a comparison with calculated modes. The energy resolution is improved beyond the thermal broadening limit and shifts induced by neighbor molecules or the position of the microscope tip are determined. Vice versa, spectra of vibrational modes are used to measure the effect of an electrical field on the energy of Yu-Shiba-Rusinov states. The method may help to further probe the interaction of molecules with their environment and to better understand selection rules for vibrational excitations.

DOI: 10.1103/PhysRevLett.129.116801

The vibrational modes of a molecule are sensitive probes of molecular bonds and their response to external parameters. They may serve as fingerprints for identification and as indicators of geometric changes. Molecular vibrations can also help elucidate processes at surfaces. In 1998, the unequivocal observation of vibrational features in data recorded with the scanning tunneling microscope (STM) was reported [1]. Like in the case of molecules in metal-oxide-metal junctions [2], the tunneling current I is modified when inelastic processes like molecular vibrations are excited. Unfortunately, the net effect on the current is usually on the order of few percent at best because the additional inelastic current is partially compensated by a reduction of the elastic current [3]. Consequently, only few molecular vibrations lead to observable signals, which typically are best discerned in d^2I/dV^2 , the second derivative of I with respect to the sample voltage V . A notable exception are data from C_{60} adsorbed to superconducting lead, where 9 modes were observed [4]. Vibronic transitions may also lead to larger changes of the tunneling conductance but detailed spectra of various modes have not been reported [5–7]. In addition, vibrational features may be resolved in single-molecule fluorescence spectroscopy with the STM [8,9].

Here, we show that sharp resonances in the density of states of paramagnetic molecules on superconductors may be used to simultaneously increase the signal amplitude and the spectral resolution of inelastic tunneling spectroscopy. The measurement concept may be introduced using energy diagrams of STM junctions (Fig. 1) between (a) two normal conductors and (b) a superconducting tip and sample. In the former case, a vibrational mode of energy $\hbar\omega$ may be excited through inelastic tunneling transitions when $V > \hbar\omega$. This leads to a minute stepwise change of the

$I(V)$ slope that becomes more readily discernible in $d^2I/dV^2(V)$. A model spectrum is displayed in Fig. 1(c). It was calculated assuming a fairly large relative change of conductance ($\eta = 10\%$) due to the inelastic processes. The peak width in d^2I/dV^2 is determined by the thermally broadened Fermi distributions so long as other instrumental effects can be neglected. In the superconducting case [Fig. 1(c)], the local densities of states of tip and sample exhibit coherence peaks and gaps around the Fermi energies. Moreover, sharp resonances within the superconducting gap of the sample may be induced by paramagnetic impurities. These Yu-Shiba-Rusinov (YSR) states are located at the energies $\pm E_{\text{YSR}}$ around the sample Fermi energy $E_F = 0$ and strongly affect the current [10–12]. In the model calculation of Fig. 1(d), the YSR peak height exceeds the background (conductance G_N outside the gap) by a factor of ≈ 20 . In some experiments, we achieved values of up to ≈ 50 . When such a resonance is the final state of a transition the inelastic current is enhanced by the same ratio. As a result, inelastic transitions prominently appear in differential conductance (dI/dV) spectra [(Fig. 1(d)] as asymmetric peaks that replicate the YSR resonances. The relative change of dI/dV due to a vibrational excitation is thus moved from the scale of a few percent [1,4] to values up to $\approx 80\%$ and the detection limit is improved by approximately 1 order of magnitude.

We investigated Pb-phthalocyanine (PbPc) on superconducting Pb(100). The experiments were performed in ultrahigh vacuum with scanning tunneling microscopes operated at 2.3 and 4.2 K. The Pb(100) substrate was prepared in vacuo by repeated cycles of Ar^+ bombardment and annealing at about 530 K. PbPc molecules were sublimated from a Knudsen cell onto the Pb substrate held at room temperature. The differential conductance dI/dV

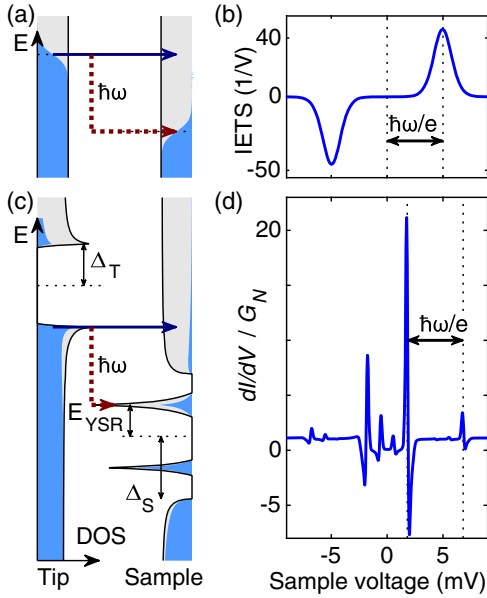


FIG. 1. (a) Schematic energy diagram of elastic (blue solid) and inelastic (red dashed) tunneling processes between normal conducting tip and sample electrodes with energy independent density of states (DOS). Both Fermi distributions (occupied states shaded in blue) are broadened by temperature. The sample voltage V is chosen to match the energy of a vibrational excitation, $eV = \hbar\omega$. (b) Second derivative d^2I/dV^2 of the current I scaled with dI/dV for the scenario in (a) (parameters $\eta = 10\%$, $\hbar\omega = 5$ meV, $T = 4.2$ K). The inelastic process gives rise to a broad peak or dip at $\pm\hbar\omega/e$. (c) Related diagram for a superconducting tip (energy gap $2\Delta_T$) and sample ($2\Delta_S$). A paramagnetic impurity induces sharp YSR states, separated by $\pm E_{\text{YSR}}$ from the Fermi level $E_F = 0$ of the sample (dotted line). V is chosen to satisfy $eV = \hbar\omega + E_{\text{YSR}} + \Delta_T$. (d) Calculated spectrum of dI/dV scaled by the conductance G_N outside the gap [η , $\hbar\omega$, and T as in (b)]. The YSR states lead to two predominant asymmetric peaks with different amplitudes at $V = \pm(E_{\text{YSR}} + \Delta_T)/e$. Tunneling of thermally excited electrons (e.g., from the upper coherence peak of the tip to the YSR state) produces minor peaks in the gap at $\pm(\Delta_T - E_{\text{YSR}})/e$. Inelastic transitions (red dashed) to the YSR states produce pairs of peaks at $\pm(\hbar\omega + E_{\text{YSR}} + \Delta_T)/e$. Their relative intensities reflect those of the YSR resonances. Their widths are much smaller than in (b) because they are not dictated by thermal broadening.

was measured using a lock-in amplifier with modulation voltages between 50 and 500 μV_{pp} at a frequency of 831 Hz.

Density functional theory (DFT) calculations were carried out for the free PbPc molecule as well as PbPc molecules adsorbed on Pb(100). We also calculated the inelastic tunneling spectrum, d^2I/dV^2 , using DFT combined with the nonequilibrium Green's function method with electron-phonon coupling taken into account using a current conserving lowest order expansion method. All calculations were performed using QUANTUMATK [13,14]. In the Supplemental Material [15], we detail the calculation methods and results.

After deposition of PbPc at ambient temperature, the molecules arrange in a square mesh with two rotational domains and lie flat on the substrate as displayed in the right inset of Fig. 2. The unit cell contains two molecules that are rotated by 8° (domain A) or 20° (domain B) with respect to each other. Although some molecules (blueish clover shaped patterns) lose the Pb ion, a majority stays intact with the ion either below or above the macrocycle.

The main experimental observation is the dI/dV spectrum (blue lower line) recorded above a Pb center. It appears flat over a wide voltage range and exhibits tall YSR resonances at ± 2 mV (left inset). Like in the case of H_2Pc [24], we find YSR states for arrays of PbPc but not for isolated molecules. A magnified view (black upper line) reveals 46 clear features positioned symmetrically around zero bias. They ride on a background that may be approximated by a superposition of a broad Lorentz-shaped resonance and the spectral signature of bulk phonons (see, e.g., Fig. S5A in the Supplemental Material at $V \approx \pm 6$ mV and $V \approx \pm 10$ mV) we observe on molecules and on pristine Pb(100). Based on the analyses presented below, we attribute the features to the excitation of molecular vibrations. The YSR resonance amplitudes depend on the bias polarity and so do the related inelastic features.

Figure 3(a) displays the low energy part of the dI/dV spectrum shifted by $E_{\text{YSR}} + \Delta_T$, with $2\Delta_T$ being the excitation gap of the tip. This shift has been applied to

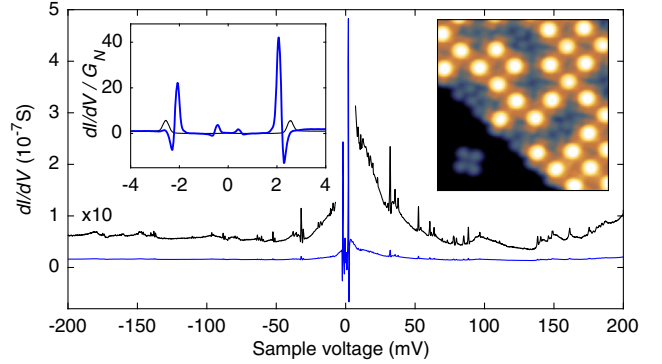


FIG. 2. dI/dV spectrum of PbPc on superconducting Pb(100). The spectrum (lower blue line) was recorded above the Pb center of a molecule within a molecular island. The most prominent spectral features are YSR resonances at ± 2 mV (see also left inset). A magnified view (multiplied by 10, black upper line) reveals a wealth of additional peaks that are due to vibration excitations. The inset to the right shows a constant-current image of molecules assembled into an island with a square mesh. Some molecules (blueish clover shaped patterns) lost their Pb ion. The majority is intact with the Pb atom imaged as a bright protrusion. The main spectrum is an average of 20 spectra recorded with an initial current of 4 nA at $V = 200$ mV and a voltage modulation of 0.5 mV_{pp} . The blue spectrum (thick line) in the inset was measured with parameters 500 pA at 5 mV and 0.05 mV_{pp} modulation, while the black (thin) curve shows $dI/dV(V)/G_N$ on a molecule without YSR states for reference.

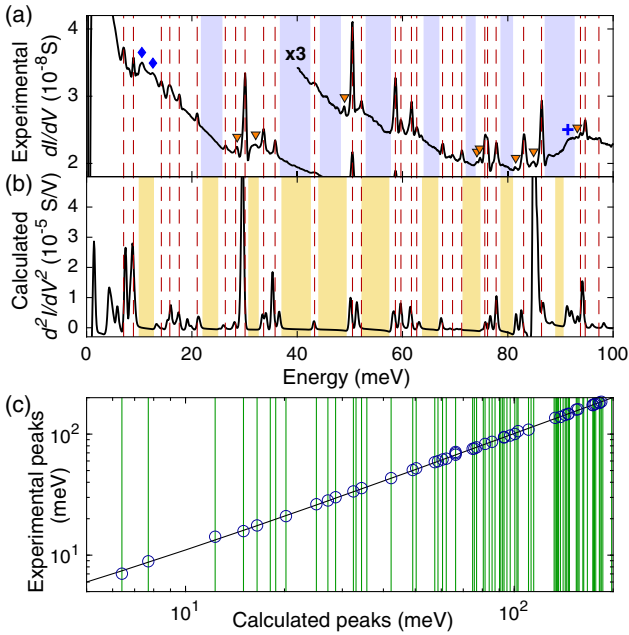


FIG. 3. Comparison of experimental and calculated spectra. (a) Low energy part of the dI/dV data from Fig. 2 shifted by the resonance position $E_{\text{YSR}} + \Delta_{\text{T}}$. Vertical dashed lines indicate peaks. Left of intense peaks, small copies are observed (orange triangles) due to thermally excited charge carriers in the tip. In addition to molecular vibrations, bulk phonons, which are also visible on pristine Pb(100), affect the spectrum at low energies. Two broader peaks (blue diamonds) were omitted from the mode assignment for this reason. A step at ≈ 90 meV (blue cross) coincides with a multippeak structure in the calculated d^2I/dV^2 . (b) Calculated spectrum of d^2I/dV^2 . Except for a 1.0 meV shift, most of the calculated peak energies match the experimental ones, thus enabling a tentative peak assignment. Shaded areas indicate gaps in the vibrational spectra. (c) Comparison of calculated peak energies (green vertical lines) with corresponding measured energies (vertical coordinate of blue circles). Logarithmic axes are used to mimic constant relative uncertainties. The black line indicates the relation $E_{\text{exp}} = E_{\text{calc}} + 1$ meV.

all experimental spectra shown as a function of energy (as opposed to sample voltage). Figure 3(b) shows a calculated spectrum of d^2I/dV^2 . Twenty-nine features are marked in the experimental data by vertical lines. We find an excellent agreement with the calculated peak energies shifted by +1.0 meV. This leads us to propose a tentative assignment of the experimental peaks to vibrational modes. Data up to 200 meV are presented in Fig. S4 in the Supplemental Material [15]. As expected, the differences between measurement and calculation are slightly larger at high energies. Nevertheless, the similarity between the calculated and measured spectra remains as indicated in Fig. 3(c). All 46 experimental modes (blue circles) match with calculated ones (green lines).

The Supplemental Material [15] presents an overview and animations of the calculated vibrational modes of a

PbPc monolayer on Pb(100). Our DFT calculations with different functionals showed that the vibrational energies are robust (Fig. S3 in the Supplemental Material [15]). The surface unit cell comprises two molecules supporting 2×171 modes, many of them being almost degenerate pairs. As expected for an array of interacting dipoles, the modes of the monolayer are blueshifted compared to those of a single adsorbed molecule (Fig. S10 in the Supplemental Material [15]), which in turn are redshifted from gas phase results because of the interaction with image charges [25,26].

In the calculated d^2I/dV^2 spectra we observe 74 peaks with intensities above an arbitrary threshold of 500 nA/V^2 corresponding to an effective cross section of $\eta \approx 0.07\%$. Several of the corresponding modes (e.g., 15, 63, 123, 205, and 239 at 6.3, 34.3, 83.9, 132.3, and 154.4 meV) exhibit the same B_1 symmetry as the two degenerate lowest unoccupied molecular orbitals (LUMOs), which are the most transmitting transport channels and, therefore, determine the electron transport [27]. Most of the intense modes correspond to experimental peaks, but some calculated modes are close in energy and thus not individually resolved in dI/dV . Presently, a more detailed analysis of the intensities is precluded by the fact that they drastically depend on the functional used and the resulting orbital energies.

At first glance it may seem surprising that electron transport through YSR states may be directly compared to transport channels involving the LUMOs. However, spatial mapping of the YSR state shows detailed similarities with the LUMOs [24]. Still some characteristics of YSR states must be considered in analyzing the experimental data, as the interaction with the tip and an electric field can change their energy and line shape. Our measurements on PbPc (Fig. S7 in the Supplemental Material [15]) and published results show that the YSR states shift, broaden, and lose intensity when the tip is brought closer to the sample [28,29]. Taking this shift of the resonances into account, we find distinct shifts of vibrational modes.

Figure 4 presents applications of the energy resolution of our method. Panel (a) shows the evolution of mode energies with the tip-sample separation. The modes near 18 and 30 meV exhibit redshifts on the order of 0.1 meV, while the modes near 58 and 86 meV undergo blueshifts of similar magnitude. The displacement patterns of the corresponding vibrational modes reveal some similarities. The redshifting modes (37/38, 55/56) involve mainly vertical atomic displacements, while the blueshifting modes (81/82, 123) are predominantly horizontal. We tentatively attribute the blueshift to the attractive force exerted by the STM tip that increases the distance between the molecule and the substrate and thereby partially reverts the adsorption-induced redshift of horizontal modes. In addition, the tip softens the potential along the surface normal and thereby induces a redshift of vertical modes.

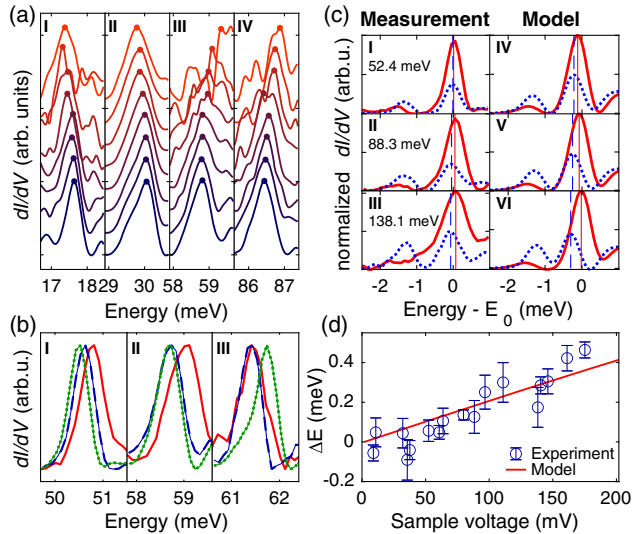


FIG. 4. Spectral changes caused by tip, neighbors, and bias polarity. (a) dI/dV spectra of a PbPc molecule recorded over a range of tip heights. For the bottom spectrum, the current feedback was disabled at $V = 200$ mV and $I = 500$ pA and the tip was brought 128 pm closer to the sample. From spectrum to spectrum the tip-sample separation was reduced by further 16 pm. A sinusoidal modulation of 0.5 mV_{pp} was used. (b) dI/dV spectra of PbPc molecules in different environments. The green dotted spectrum was recorded on a molecule with PbPc on nearest neighbor (NN) and next nearest neighbor (NNN) sites. The blue dashed (red solid) curve shows data where Pb was absent from NN (NN and NNN) molecules. (c) Left column: Experimental dI/dV data of excitations at 52.5, 88.3, and 138.1 meV measured at positive (red solid) and negative (blue dotted) V . $E_0 = E_{\text{YSR}} + \Delta_T + \hbar\omega$. The main peaks are due to tunneling from the occupied (unoccupied) coherence peak of the tip to the unoccupied (occupied) YSR state at $V > 0$ ($V < 0$). Thermally excited charge carriers lead to a minor peak in each spectrum. The positions of the main peaks (dashed vertical lines) do not exactly coincide and separate with $|V|$ in a linear fashion. The relative heights of the major and minor peaks also change. Right column: dI/dV calculated with a model that considers a voltage dependence of the YSR states reproduces the experimental data. (d) Polarity induced differences of peak positions evaluated from various excitations. A model presented in the Supplemental Material reproduces the observed linear relation (Eq. 6). Experimental parameters are identical to those in Fig. 2.

Next, we reverse the roles of YSR states and vibrational excitations. As the voltage between the tip and the sample may gate the molecule, the energy and peak height asymmetry of YSR states could be bias dependent. In contrast to elastic tunneling processes, which probe YSR states at voltages close to zero, the vibration induced copies of the YSR resonances appear at higher voltages and therefore provide access to a possible gating effect. Figure 4(c) shows the spectra of three vibrational excitations at positive (red solid line) and negative (blue dotted line) voltages. Each excitation gives rise to a pair of peaks at both polarities, the peak closer to zero bias being due to

thermally excited electrons (holes) in the coherence peaks of the tip above (below) E_F . Toward higher excitation energies, the peaks separate in a linear fashion (Fig. 4(d), circles). The changes in peak positions and the shape of the inelastic signatures are well reproduced within a Bogoliubov-de Gennes model (Fig. 4(d), line). To calculate inelastic tunneling spectra, the bias dependent density of states of the sample around E_F is obtained using a Green's function approach that takes into account a constant potential scattering W and an exchange coupling J , which depends linearly on the voltage. The observed shift may be understood as follows. At $V < 0$, the LUMO is lowered relative to E_F of the sample, its occupation increases, the YSR state moves deeper into the superconductor gap, and finally the peak height asymmetry is enhanced.

The interaction between a molecule and its local environment may also be addressed. Figure 4(b) and Fig. S6 in the Supplemental Material [15] show spectra of PbPc molecules surrounded by PbPc molecules on nearest neighbor (NN) and next nearest neighbor (NNN) sites (green dotted). When the Pb ions are removed from either NN molecules (blue dashed) or both, NN and NNN molecules (red solid line), the vibrational modes observed on the center PbPc undergo small but clearly resolved shifts. Three segments from spectra in Fig. 4(b) illustrate diverse evolutions. Some modes shift continuously to lower (Fig. 4(b)-I) or higher (Fig. S6 in the Supplemental Material [15]) energies as the number of neighbors with Pb increases. In other cases (Fig. 4(b)-II), NNN PbPc induces a substantial redshift that is not further affected by NN Pb ions. For the vibrations shown in Fig. 4(b)-III, NNN PbPc molecules are required to produce a substantial blueshift.

In summary, taking advantage of YSR states, the detection limit of vibrational spectroscopy with the STM is improved and the energy resolution is pushed beyond the thermal limit. Such resonances may be expected from molecules that carry a spin, be it due to intrinsic molecular properties or charge transfer involving the environment. While modeling of the vibrational mode energies is fairly accurate, the inelastic intensities will require further attention.

*Corresponding author.
 weismann@physik.uni-kiel.de

†Corresponding author.
 berndt@physik.uni-kiel.de

- [1] B. C. Stipe, M. A. Rezaei, and W. Ho, *Science* **280**, 1732 (1998).
- [2] R. C. Jaklevic and J. Lambe, *Phys. Rev. Lett.* **17**, 1139 (1966).
- [3] N. Lorente and M. Persson, *Phys. Rev. Lett.* **85**, 2997 (2000).
- [4] K. J. Franke and J. I. Pascual, *J. Phys. Condens. Matter* **24**, 394002 (2012).

- [5] B. Doppagne, M. C. Chong, E. Lorchat, S. Berciaud, M. Romeo, H. Bulou, A. Boeglin, F. Scheurer, and G. Schull, *Phys. Rev. Lett.* **118**, 127401 (2017).
- [6] F. Matino, G. Schull, F. Köhler, S. Gabutti, M. Mayor, and R. Berndt, *Proc. Natl. Acad. Sci. U.S.A.* **108**, 961 (2011).
- [7] F. Schwarz, Y. F. Wang, W. A. Hofer, R. Berndt, E. Runge, and J. Kröger, *J. Phys. Chem. C* **119**, 15716 (2015).
- [8] X. H. Qiu, G. V. Nazin, and W. Ho, *Science* **299**, 542 (2003).
- [9] Z.-C. Dong, X.-L. Guo, A. S. Trifonov, P. S. Dorozhkin, K. Miki, K. Kimura, S. Yokoyama, and S. Mashiko, *Phys. Rev. Lett.* **92**, 086801 (2004).
- [10] A. Yazdani, B. A. Jones, C. P. Lutz, M. F. Crommie, and D. M. Eigler, *Science* **275**, 1767 (1997).
- [11] M. Ruby, F. Pientka, Y. Peng, F. von Oppen, B. W. Heinrich, and K. J. Franke, *Phys. Rev. Lett.* **115**, 087001 (2015).
- [12] C. Rubio-Verdú, J. Zaldívar, R. Žitko, and J. I. Pascual, *Phys. Rev. Lett.* **126**, 017001 (2021).
- [13] QuantumATK version T-2022.03, Synopsys QuantumATK (www.synopsys.com/silicon/quantumatk.html).
- [14] S. Smidstrup *et al.*, *J. Phys. Condens. Matter* **32**, 015901 (2020).
- [15] See Supplemental Material at <http://link.aps.org/supplemental/10.1103/PhysRevLett.129.116801> for supplemental text, Figs. S1–S9, Tables S1 and S2, and animations of Modes 1–302, which includes Refs. [16–23].
- [16] J. P. Perdew, K. Burke, and M. Ernzerhof, *Phys. Rev. Lett.* **77**, 3865 (1996).
- [17] J.-T. Lü, R. B. Christensen, G. Foti, T. Frederiksen, T. Gunst, and M. Brandbyge, *Phys. Rev. B* **89**, 081405(R) (2014).
- [18] T. Gunst, T. Markussen, K. Stokbro, and M. Brandbyge, *Phys. Rev. B* **93**, 245415 (2016).
- [19] T. Frederiksen, M. Paulsson, M. Brandbyge, and A.-P. Jauho, *Phys. Rev. B* **75**, 205413 (2007).
- [20] J. Heyd, G. E. Scuseria, and M. Ernzerhof, *J. Chem. Phys.* **118**, 8207 (2003).
- [21] J. Heyd, G. E. Scuseria, and M. Ernzerhof, *J. Chem. Phys.* **124**, 219906 (2006).
- [22] S. L. Dudarev, G. A. Botton, S. Y. Savrasov, C. J. Humphreys, and A. P. Sutton, *Phys. Rev. B* **57**, 1505 (1998).
- [23] M. E. Flatté and J. M. Byers, *Phys. Rev. B* **56**, 11213 (1997).
- [24] J. Homborg, A. Weismann, R. Berndt, and M. Gruber, *ACS Nano* **14**, 17387 (2020).
- [25] M. Scheffler, *Surf. Sci.* **81**, 562 (1979).
- [26] M. Endlich, A. Michl, J. Hildisch, S. Müller, and J. Kröger, *J. Phys. Chem. C* **120**, 11490 (2016).
- [27] M. Paulsson, T. Frederiksen, H. Ueba, N. Lorente, and M. Brandbyge, *Phys. Rev. Lett.* **100**, 226604 (2008).
- [28] L. Farinacci, G. Ahmadi, G. Reecht, M. Ruby, N. Bogdanoff, O. Peters, B. W. Heinrich, F. von Oppen, and K. J. Franke, *Phys. Rev. Lett.* **121**, 196803 (2018).
- [29] S. Kezilebieke, M. Dvorak, T. Ojanen, and P. Liljeroth, *Nano Lett.* **18**, 2311 (2018).